Supplementary Information (SI)

Atomic Layer Deposition of Sn-doped Germanium Diselenide for As-free Ovonic Threshold Switch with Low Off-current

*Byongwoo Park,[†a] Jeong Woo Jeon,[†a] Woohyun Kim,[a] Wonho Choi,[a] Gwang Sik Jeon,[a] Sangmin Jeon,[a] Sungjin Kim,[a] Chanyoung Yoo,[b] Junyoung Lim,[c] Yonghun Sung,[c] David Ahn,[c] and Cheol Seong Hwang[*a]*

[a]*Department of Materials Science and Engineering and Inter-University Semiconductor Research Center, Seoul National University, Seoul, 08826, Republic of Korea.*

[b]*Department of Materials Science and Engineering, Hongik University, Seoul, 04066, Republic of Korea*

[c]*SK hynix Inc., Icheon, Gyeonggi, 17336, Republic of Korea*

[†]These authors contributed equally.

**E-mail: cheolsh@snu.ac.kr*

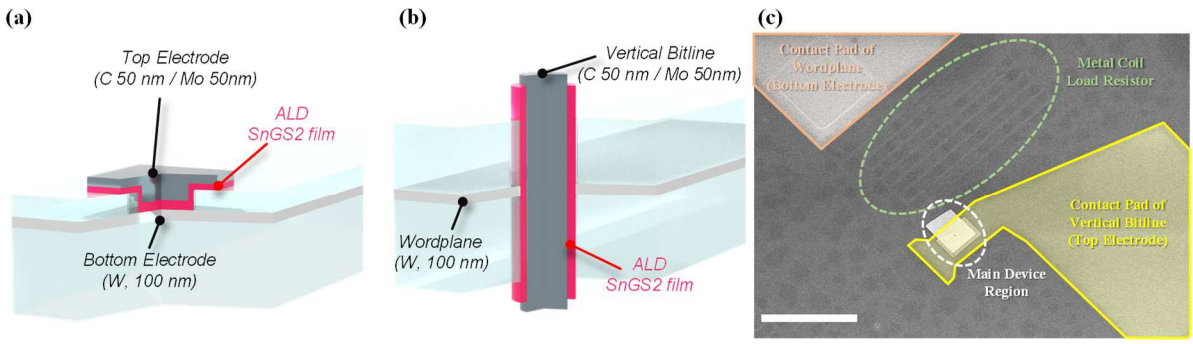

Figure S1. Schematic diagram of (a) planar and (b) vertical OTS devices, illustrating the main device region. (c) The bird's-eye view image of the OTS device, highlighting the main device region, load resistor, and the contact pad used for the electrical measurement. Scale bar, 50 μm.

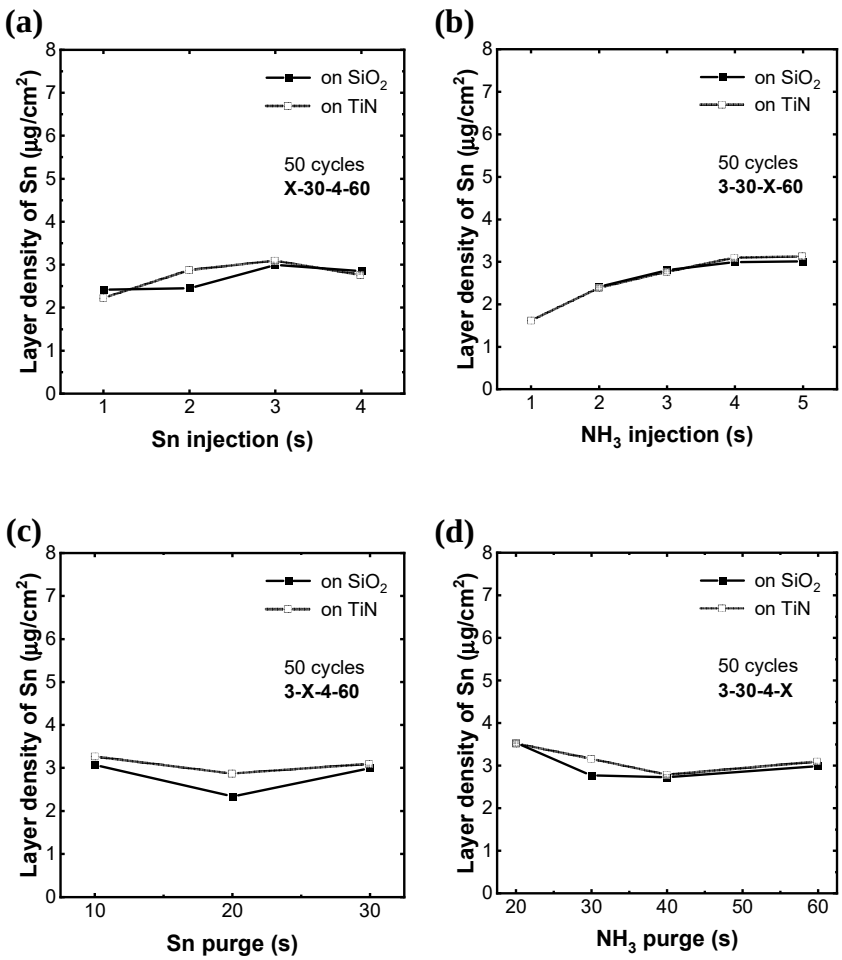

Figure S2. Variation in layer density of Sn in the SnN_x film at 110 °C depending on the (a) injection times of TDMA-Sn, (b) injection times of NH_3, (c) purge times of TDMA-Sn, and (d) purge times of NH_3.

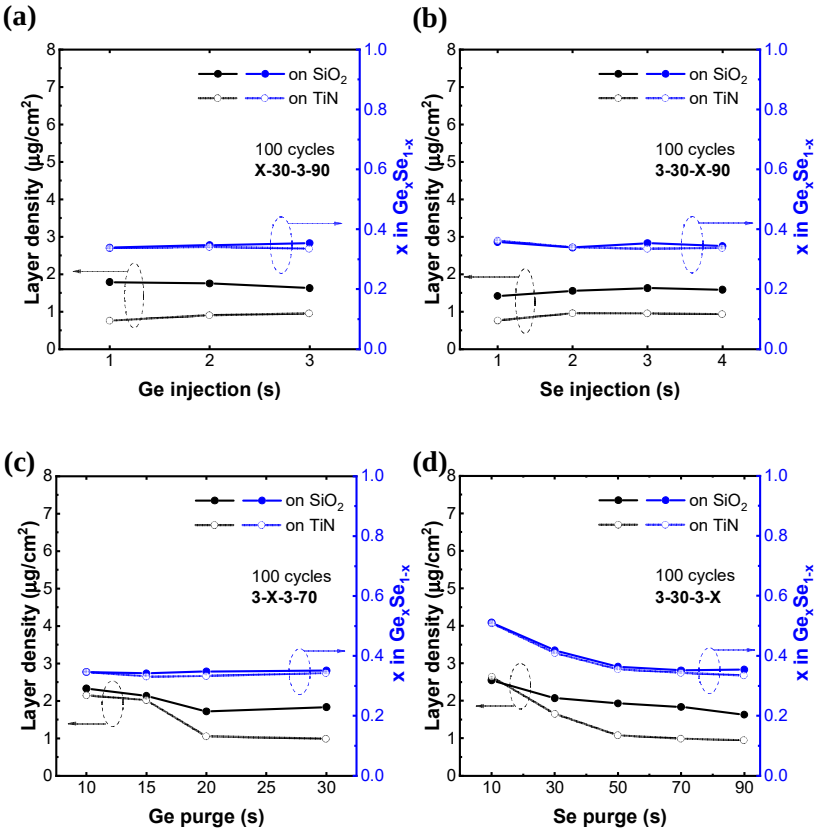

Figure S3. Saturation behavior of the $GeSe_2$ film at 110 °C depending on the (a) injection times of TDMA-Ge, (b) injection times of BTMS-Se with NH_3, (c) purge times of TDMA-Ge, and (d) purge times of BTMS-Se with NH_3.

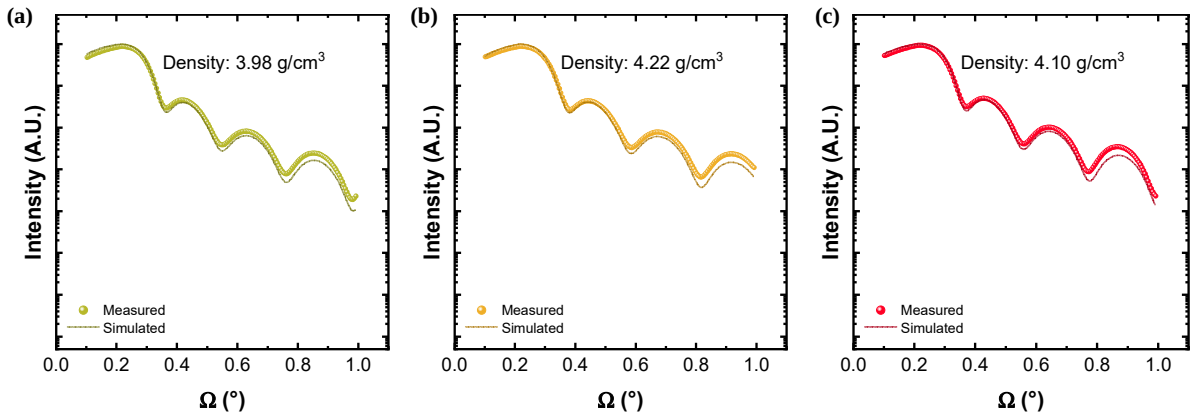

Figure S4. XRR measurement results of the ALD SnGS2 films for different subcycle ratios. (a) [1-10], (b) [1-5], and (c) [2-5]. The number of supercycles of each film is 18, 30, and 24, respectively.

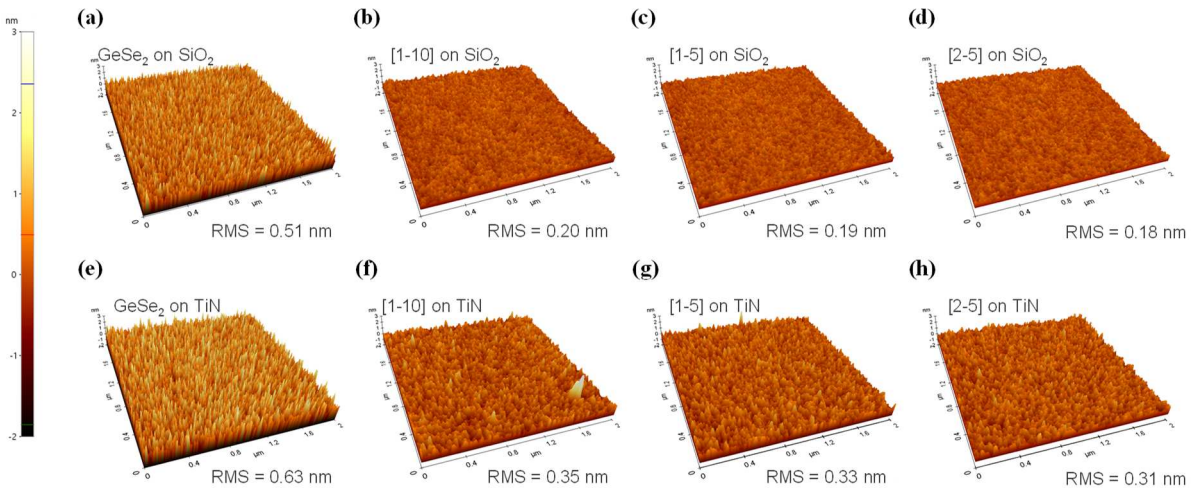

Figure S5. AFM measurement results of the 15 nm-thick-$GeSe_2$ and SnGS2 films on (a-d) SiO_2 and (e-h) TiN substrates.

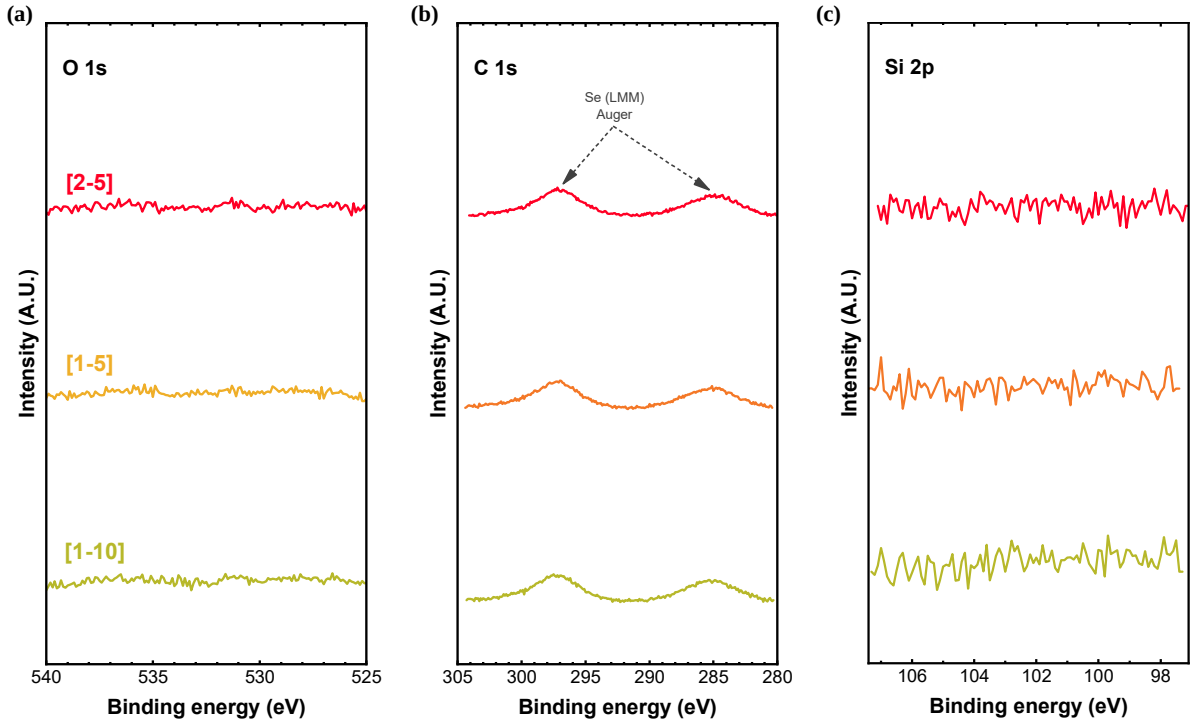

Figure S6. XPS spectra of the ALD SnGS2 films. (a) O 1s, (b) C 1s, and (c) Si 2p peaks, respectively.

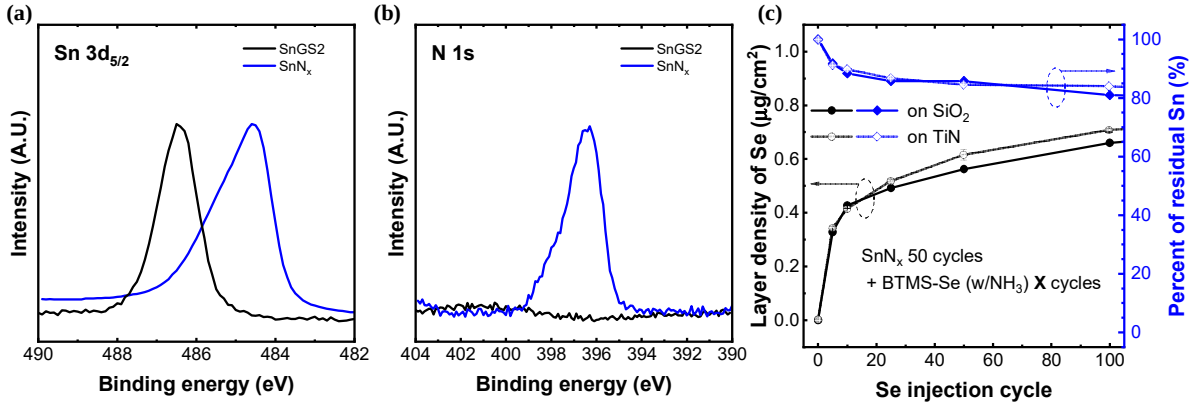

Figure S7. XPS spectra comparison of SnN_x (black) and SnGS2 (blue) films. (a) Sn $3d_{5/2}$ and (b) N 1s peak, respectively. The spectra shown for the SnGS2 films correspond to those deposited with SnN_x and $GeSe_2$ subcycles of 2 and 5, respectively. (c) Variation in the layer density of Se as a function of the number of BTMS-Se and NH_3 co-injection cycles after the deposition of 50 cycles of SnN_x.

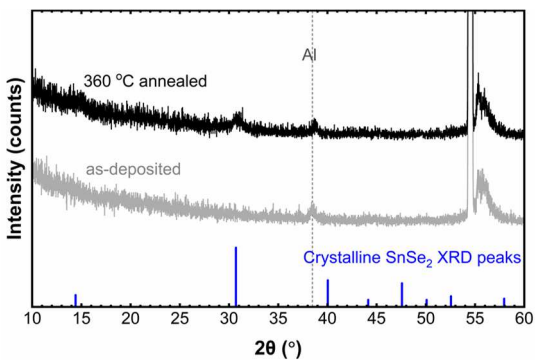

Figure S8. GIXRD measurement results to confirm the crystallization temperature of highly Sn-doped SnGS2 film. The subcycles of SnN_x and $GeSe_2$ were 3 and 5, respectively, and the film thickness was 15 nm. The blue lines indicate the XRD peak positions corresponding to crystalline $SnSe_2$.

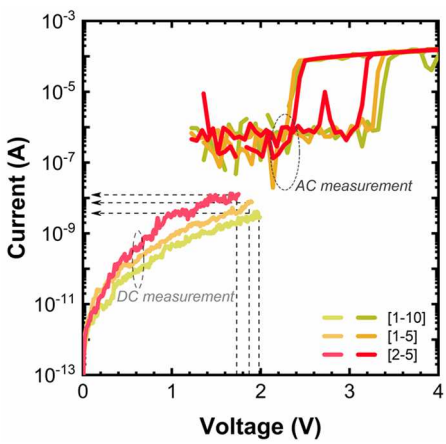

Figure S9. Characteristic *I-V* data of different SnGS2 OTS planar devices. The data for the subthreshold voltage range were measured by DC signal, and AC of triangular pulses measured the threshold switching range.

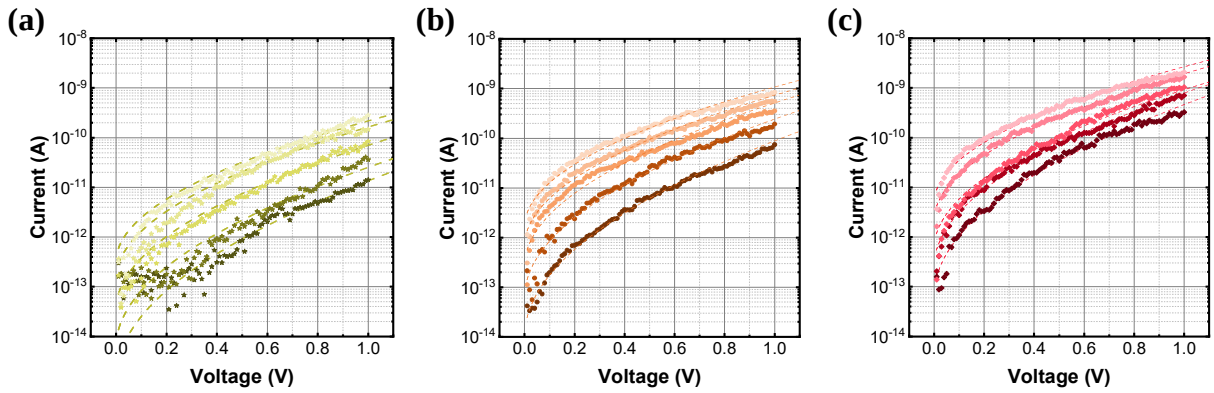

Figure S10. Temperature-dependent *I-V* curves of an OTS device based on SnGS2 after the forming state. The symbols and solid lines represent the measured data and the model fitting results, respectively. The following symbols represent the subcycle ratio of SnGS2: (a) [1-10] (star), (b) [1-5] (circle), and (c) [2-5] (diamond). The measurements were taken in 30 °C steps, from 25 °C (darkest symbols) to 145 °C (lightest symbols), as indicated by the color gradient of the symbols.

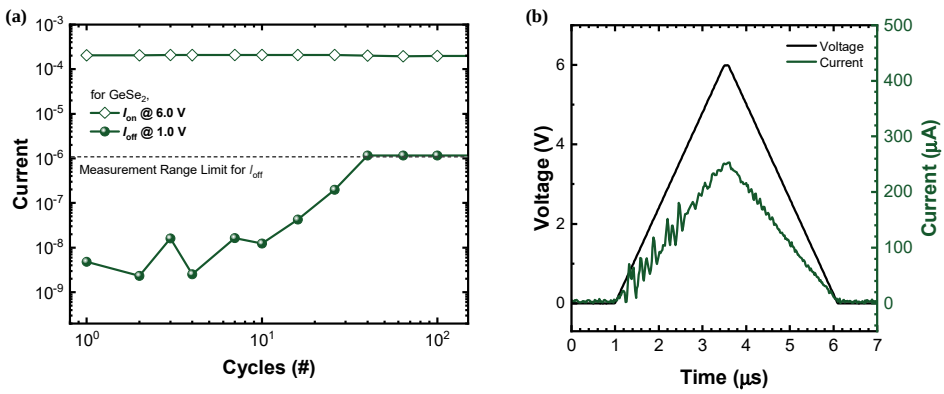

Figure S11. Electrical measurement results of the planar OTS device using the $GeSe_2$ film. (a) Pulsed endurance test results during 100 cycles. (b) Electrical behavior during the triangular pulse application after the cyclic endurance test. The device no longer exhibited the typical OTS behavior.

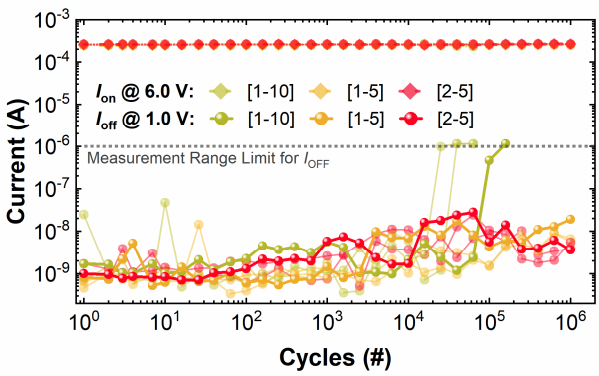

Figure S12. Pulsed cyclic endurance results of 3 different devices for each SnGS2 composition.

Table S1. Benchmark of As-free OTS electrical characteristics based on Se-rich Ge_xSe_{1-x} films.

OTS material	Device structure	Deposition method	Thickness (nm)	Forming voltage, V_f (V)	Threshold voltage, V_t (V)	Endurance	Selectivity	Off current density, J_{off} (A/cm^2)	Reference
Ge_4Se_6	Planar	Sputtering	30	~ 10	2.8	< 10^5	< 10^5	~ 6.0	[1]
$Ge_{3.3}Se_{2.2}S_{4.5}$	Planar	Sputtering	15	6.1	3.7	> 10^8	~ 8.3 x 10^4	42	[2]
$Ge_{3.3}Se_{5.5}S_{1.2}$				4.8	3.0	> 10^7	~ 3.2 x 10^4	1.1 x 10^2	
Ge_3Se_7	Planar	Sputtering	-	-	4.0	< 10^2	10^3	5.7 x 10^{-3}	[3]
$Ge_{2.8}Se_{6.4}N_{0.8}$					3.4	< 10	5 x 10^3	3.8 x 10^{-3}	
$Ge_{2.4}Se_{6.6}Sb_{2.0}$					2.1	< 10^2	13	19	
$Ge_{2.3}Se_{5.1}Sb_{2.0}N_{0.8}$					2.2	> 10^6	10^4	3.4 x 10^{-3}	
$GeSe_2$	Planar	ALD	10	3.4	1.9	< 10^3	5 x 10^2	1.0 x 10^4	[4]
$Ge_5Se_3S_2$				4.3	3.2	~ 10^6	3.3 x 10^3	1.5 x 10^3	
[1-10]	**Planar**	**ALD**	**15**	**8.8**	**4.0**	**~ 10^5**	**> 10^5**	**0.6**	**This work**
[1-5]				**8.6**	**3.7**	**> 10^6**		**1.0**	
[2-5]				**8.3**	**3.5**	**> 10^6**		**1.5**	
[2-5]	**Vertical**			**8.4**	**3.5**	-		**1.6**	

[1] B. Song, H. Xu, S. Liu, H. Liu, Q. Liu and Q. Li, *Appl. Phys. A Mater. Sci. Process.*, 2019, **125**, 1–6.
[2] M. Lee, S. Lee, M. Kim, J. Lee, C. Kwon, C. Won, T. Kim, S. Lee, S. Cho, S. Na, S. Park, K. Yoon, H. Kim and T. Lee, *J. Alloys Compd.*, 2024, **973**, 172863.
[3] A. Verdy, G. Navarro, V. Sousa, P. Noe, M. Bernard, F. Fillot, G. Bourgeois, J. Garrione and L. Perniola, in *2017 IEEE International Memory Workshop (IMW)*, IEEE, 2017, pp. 1–4.
[4] S. Jun, S. Seo, S. Park, T. H. Kim, M. Lee, S. M. Hong, T. Kim, S. Chung, T. Lee, M. Kim and H. Kim, *J. Alloys Compd.*, 2023, **947**, 169514.